JOURNAL OF MATERIALS SCIENCE 28 (1993) 4104–4112

Preparation and characterization of radio-frequency-sputtered $Ba_2Si_2TiO_8$ thin films

YI LI, P. M. KAWA, W. V. YOUDELIS
Engineering Materials Group, Mechanical Engineering Department, University of Windsor, Windsor, Ontario, Canada N9B 3P4
B. S. CHAO
Energy Conversion Devices, Incorporated Troy, MI 48084, USA
H. YAMAUCHI
Division II, International Superconductivity Technology Center, 10-13 Shinonome, 1-Chome, Koto-Ku, Tokyo 135 Japan

Radio-frequency-sputtered barium titanium silicate (BST, $Ba_2Si_2TiO_8$) thin films were grown on crystalline Si (1 0 0) substrates and were characterized using wavelength-dispersive spectrometry (WDS), X-ray diffraction (XRD), optical microscopy (OM) and scanning electron microscopy (SEM), and diagonal techniques for dielectric properties. The chemical compositions of the films increasingly deviated from stoichiometry with film thickness. At the initial stage of deposition the grain configuration is dependent on the Si substrate texture. XRD analysis indicates that the BST films deposited at an optimum substrate temperature of 845 °C were strongly *c*-axis oriented, and that the film orientation is manipulated by substrate temperature and supersaturation. The corresponding film-growth rate in the direction normal to the film surface at 845 °C was 1.95 nm min^{-1} at the initial stage, and decreased with sputtering time. The as-deposited films have a room-temperature bulk resistivity of $1.8 \times 10^7\ \Omega$ m in the direction of thickness and an isotropic surface resistivity of $1.5 \times 10^3\ \Omega$ m. The high-frequency relative dielectric constant, 0.05 at frequencies higher than 9 MHz, is lower than that of many typical piezoelectric materials. The high-frequency impedance character is typical of piezoelectric materials, giving a minimum impedance frequency of 9.0 MHz and a serial resonant frequency at about 9.5 MHz.

1. Introduction

Barium titanium silicate (BST), $Ba_2Si_2TiO_8$, a functional ceramic belonging to the p4bm space group and having lattice constants $a = b = 0.852$ nm and $c = 0.521$ nm [1, 2], is piezoelectric due to its asymmetrical crystal structure, high tetragonality, c/a, of 0.61, and large unit-cell spontaneous dipole moment of 1.14×10^{-26} C m. BST possesses a high piezoelectric coupling constant, K^2, [3–5]; a small temperature coefficient of delay (TCD) [4, 5]; and a low phase velocity [4]. These properties are intermediate between the well-known piezoelectric materials, $LiNbO_3$ and $LiTaO_3$ [6, 7], and make BST a potential temperature-compensated material for surface-acoustic-wave (SAW) devices [8]. BST attracts special attention because its calculated TCD is equal to zero and its other useful SAW properties for its thin films reported by Yamauchi *et al.* [9]. To fabricate a qualified BST thin film for SAW devices, the crystal grains of the film should be highly *c*-axis oriented [10]. The required minimum film thickness of 2.0 μm can be determined by the frequency constant [9].

The formation of amorphous BST thin films on NaCl crystals, glasses, fused quartz, mica, and Si (1 0 0) substrates by means of the diode and triode sputter methods [11, 12] and the formation of *c*-axis-oriented BST films deposited on Si (1 0 0) substrates by a radio-frequency (r.f.) sputter method [13] has been reported by Yamauchi and coworkers. The film quality was generally poor. The *c*-axial orientation of the films deposited on Si (1 0 0) substrates at 725 °C tended to deteriorate quickly with deposition time and to change into a randomly oriented structure. Recent work has shown that highly *c*-axis-oriented BST thin films can be prepared with a thickness up to 2.8 μm grown on Si (1 0 0) substrates. Grain and film-growth kinetics for BST films have been studied [14, 15]. It was found that the substrate texture plays an important part in determining the crystallographic configuration of the BST film [16], and that up to six different film orientations can be obtained by varying the substrate temperature [17].

For a crystalline film, the grains or crystallites are formed by independent nucleation and growth processes particularly oriented and spaced with respect to one another [18]. At any time there are probably several orientations existing and competing with each other, and only the orientation with a fast nucleation

0022–2461 © 1993 Chapman & Hall

rate is favoured. The conditions for orientation formation have been extensively studied, and atomic-nucleation [19] and capillarity [20, 21] theories are involved to explain various orientation behaviours. According to the capillarity theory, at a fixed temperature and a fixed evaporation rate, the competition of any two orientations could be described by using the ratio of the nucleation rate for nuclei of the two orientations, J_1 and J_2, given by

$$\frac{J_2}{J_1} = \frac{C_2}{C_1}\exp\left(\frac{\Delta G_1^* - \Delta G_2^*}{kT}\right) \quad (1)$$

where k is the Boltzmanns constant, C is a weakly temperature-dependent constant, ΔG^* is the critical free energy for formation of a nucleus and is given by a function of the surface energy and interfacial energy, A, and the free-energy change per unit volume, Ω, when the condensate is formed from the supersaturated monomer population, ΔG_v, as $\Delta G^* = A/(\Delta G_v)^2$. ΔG_v is related to the supersaturation p/p_e by $\Delta G_v = -(kT/\Omega)\,\ln(p/p_e)$, where p and p_e are the vapour pressures of the sputtering source and equilibrium vapour pressure of the adatoms, respectively. Then the exponential part of Equation 1 is

$$\frac{\Delta G_1^* - \Delta G_2^*}{kT} = \frac{\Omega^2(A_1 - A_2)}{(kT)^3\left[\ln\left(\frac{p}{p_e}\right)\right]^2} \quad (2)$$

Thus the capillarity model assumes that the degree of an orientation is a function of the interfacial energy, A, substrate temperature, T, and the supersaturation p/p_e. For example, a nucleus with a lower interfacial energy A_2 will have higher nucleation rate J_2. The predominant nucleation rate must be maintained by a corresponding substrate temperature and a proper supersaturation.

In this study, the preparation method of the highly c-axis-oriented BST films is introduced. The film chemical compositions and crystal structures are analysed to show the influences of three main experimental conditions (i.e. substrate texture, substrate temperature and supersaturation) on the film qualities. The film dielectric properties and related analysis are also presented.

2. Experimental procedure

BST thin films were deposited on a Si substrate using a magnetron-assisted, r.f.-triode sputtering assembly. The base pressure in the vacuum chamber was 2.6×10^{-5} Pa and then back-filled to 0.16–0.20 Pa with Ar. The depositions were carried out under conditions of 4 cm source–substrate distance, 50 W r.f. power, and 0.16–0.20 Pa Ar pressure.

A BST ceramic target, 1 inch in diameter, was formed through the following reaction

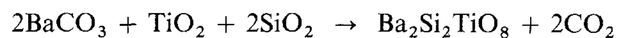

$$2BaCO_3 + TiO_2 + 2SiO_2 \rightarrow Ba_2Si_2TiO_8 + 2CO_2$$

Reagent-grade barium carbonate, titanium dioxide and silicon dioxide were used as reactants, which were dried separately at 400 °C for 4 h and then weighed for determination of stoichiometric weights. The weighed powders were mixed in a ball mill and ground for 40 h, followed by grinding for 2 h using a mortar and a pestle. The ground powder was divided into small portions and pressed into discs under a pressure of 6 MPa before calcination at 1000 °C for 13 h. The calcined discs were powdered again for 3 h pressed into discs at 60 MPa, and then sintered at 1260 °C for 6 h.

An n-type single crystalline Si (1 0 0) wafer was used as the substrate (25 × 25 mm). The silicon wafers were cleaned by acetone and ethanol in an ultrasonic cleaner, followed by etching in a dilute HF solution (1:40 in de-ionized water). The target was mounted at the sputtering source 4 cm away from the substrate. The substrate was heated with a tantalum-wire heater at a distance of 4 mm [15]. Alumina plates were used to support the heater and to insulate the heater. A digital thermometer (Model 2168A, Omega Engineering, Inc.), with a 1 °C resolution, was used to monitor the substrate temperature, using a chromel–alumel thermocouple mounted at the same level as the Si substrate. The substrate temperature, T_s was varied from 750 to 1100 °C.

The chemical composition of the BST ceramic target and thin films were measured using a wavelength-dispersive spectrometry (WDS) technique. The experimental error in the analysis is ± 5%. The morphology of the as-deposited films was studied using optical microscopy (OM) and scanning electron microscopy (SEM). The crystal structure of the films was determined by X-ray diffractometry, using CuK_α radiation. The orientations of the thin films are reported as an X-ray-peak-intensity ratio of the (0 0 1) reflection to the (2 1 1) reflection, $I(0\,0\,1)/I(2\,1\,1)$; the (2 1 1) reflection is the strongest reflection of the randomized BST crystallites [22].

The surface resistivity of BST films were measured by means of a collinear four-point-probe arrangement [23]. The direct current (d.c.) voltage between the probes and the d.c. electric current between the inner probes were monitored by a 3800 A Digital Multimeter and an 8842 A Fluke Multimeter, respectively. The resistivities of the films were calculated from the potential drop across the inner probes, the current flow through the probes, and the width between the probes [24]. The bulk resistivity and the high-frequency characteristics of the films were carried out on a Au-BST-Si electrode system, which was formed by the deposition of circular gold electrodes, 8 mm in diameter and 250 nm in thickness, onto the as-deposited BST films. The gold layer and the Si substrate were used as electrodes because of the oxide-free nature of the gold and the low resistivity of the Si substrate, approximately 5×10^{-3} to 2×10^{-2} Ω m. The d.c. resistivity in the direction of the film thickness was measured with positive and negative biases under electric field strengths ranging from 0.05 to 3.0 kV cm^{-1}. The measurement of the high-frequency capacitance, C, the dielectric loss, D (defined as the ratio of the real power to the reactive power of the electrode system), the impedance, Z, and the phase angle of the impedance was performed in a frequency range from 1 to 1000 MHz, using a HP 4191 RF

Impedance Analyser. The relative dielectric constant, ε_r, was calculated from the film capacitance, $C = \varepsilon_0 \varepsilon_r S/d$, where ε_0 is the vacuum dielectric constant, and S and d are the area and thickness of the Au–BST–Si capacitor, respectively.

3. Results and discussion

3.1. In-depth-chemical-composition profile

The BST target fabricated for the film deposition is a pale green, polycrystalline ceramic disc. The BST film deposited on a Si (100) substrate at 845 °C is a smooth, glossy and dark-blue film. The chemical compositions in atomic percentages for the BST target and thin films with thickness of 0.7, 1.05, and 2.8 μm, deposited at 845 °C, are given in Table I. The stoichiometric composition of BST is also listed in Table I for comparison. The composition of the BST target is very close to the stoichiometric composition. The minimum and maximum relative errors for the target composition are + 0.002 for Ba and + 0.07 for Ti, respectively. The shortage of Si is probably caused by the loss of the very fine and light-weight powders of SiO_2 during the grinding. The extra Ti is due to the shortage of other elements. Table I shows that the film compositions deviate from those of the target, and that the deviation increases with film thickness. For the 30 h sputtered 2.8 μm thick film, the elements O and Ba are short by − 11.0% and − 33.8%, respectively. Vacuum sputter is a complicated process, involving numerous chemical and physical mechanisms in three material-transport processes: (i) emission from the target, (ii) transport between the target and the substrate, and (iii) reaction at the substrate [25, 26]. The changing stoichiometry of the BST films could be a result of a change in the stoichiometry of the sputtered target surface, or a result of the preferred scattering of large-size ions, such as O^{-2} and Ba^{+2}, in the interval between the target and the substrate. Different re-sputter rates of elements at the film surface may also account for the off-stoichiometry of the films. The deviation in chemical composition was also found in the r.f.-sputtered, amorphous BST films [12]. An effort to modify the film composition has been made by altering the target composition [13, 27], but no improvement was found. This may suggest a large-sized target, and hence a high flux of the sputtered species, and a short sputtering time give a better film composition.

The deviation in film stoichiometry may account for the formation of phases other than BST in the films, which is difficult to identify in the XRD spectra of the films, probably due to their small amount or due to their short-range ordered structure located at BST-grain boundaries. After heat treatment of the as-deposited BST films at 1000 °C for longer than 30 min, some of the X-ray peaks of the off-BST phases, even though very weak, could be found in the XRD spectra, such as the peak at $2\theta = 31.6°$ originating from the (1 0 1) plane of the tetragonal $BaTiO_3$ [28].

3.2. Dependence of film morphology on substrate texture

BST has a tetragonal crystal structure with equal lattice constants a and b, and a shorter side c in its unit lattice. Fig. 1 is an optical photomicrograph taken from a discontinuous BST film deposited at 845 °C for 8 min, which displays tetragonal-like grains grown on a Si (1 0 0) substrate in the initial stage of deposition. The edges of all the grains are parallel to the (0 1 0) and (0 0 1) directions of the Si substrate reducing the interfacial energy of the interface between the deposits and the substrates, and the corners of the grains are rounded due to surface tension. The (0 0 1) orientation is dominant at 845 °C because the BST (0 0 1) plane has both the highest planar atomic density among all the atomic planes and the lowest interfacial energy when it grows on the Si (1 0 0) substrate, and it is thus most stable at the lowest substrate temperature in the following series of four different orientations observed in the substrate temperature region from 786 to 899 °C: (0 0 1), (1 1 1), (3 2 0), and (4 1 0) (see Equation 2) [17].

The different grain sizes in Fig. 1 imply a random incubation period for the nucleation process followed by the grain-growth process. In the later stage of deposition, grains touch and grow without significantly

TABLE I Chemical compositions of BST targets and thin films

Specimen	Source of data	Composition (at %)			
		O	Si	Ti	Ba
$Ba_2Si_2TiO_8$ Target	Stoichiometry	61.54	15.38	7.96	15.38
	Analysis	61.31 ± 3.07 (− 0.3%)[a]	15.01 ± 0.75 (− 2.0%)[a]	8.26 ± 0.41 (7.0%)[a]	15.42 ± 0.70 (0.2%)[a]
Thin Film	Analysis (0.70 μm)[b]	61.27 ± 3.06 (− 0.4%)[a]	15.86 ± 0.79 (3.1%)[a]	12.95 ± 0.65 (68.4%)[a]	9.92 ± 0.50 (− 35.5%)[a]
	Analysis (1.05 μm)[b]	60.82 ± 3.04 (− 1.1%)[a]	17.92 ± 0.90 (16.5%)[a]	12.16 ± 0.61 (58.1%)[a]	9.10 ± 0.46 (− 40.8%)[a]
	Analysis (2.80 μm)[b]	54.74 ± 2.74 (− 11.0%)[a]	19.42 ± 0.97 (26.2%)[a]	12.16 ± 0.61 (103.6%)[a]	10.17 ± 0.51 (− 33.8%)[a]

[a] The error (relative error) of the atomic percentage of the element in ceramic targets and thin films relative to the stoichiometric atomic percentage of the element in BST.
[b] Thickness of the film.

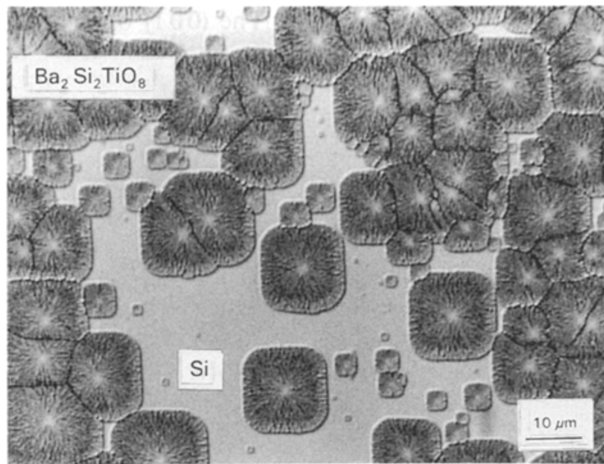

Figure 1 Optical photomicrograph taken from a BST film, deposited on a Si (1 0 0) substrate at 845 °C for 8 min, displaying the crystal morphology of BST grains.

changing their individual shapes. In various film-formation processes, the different deposit-coalescence behaviours depend on the balance of the surface energy of the deposit and the interfacial energy of the interface between the deposit and the substrate [20, 21]. The non-liquid-like coalescence of BST grains grown on the single-crystal Si may be attributed to a strong interaction between the BST (0 0 1) plane and the Si (1 0 0) plane [16]. One of the characteristics of the non-liquid-like coalescence is the fast lateral growth rate of the grains in the direction parallel to the substrate surface. Recent studies on the BST grain and film-growth kinetics [14, 15] reported an initial lateral grain-growth rate of 0.77 $\mu m\,min^{-1}$ for the films deposited on Si (1 0 0) substrates at 845 °C, which is higher than the film-growth rate in the direction normal to the substrate by two orders of magnitude.

Another significant characteristic of the non-liquid-like coalescence is the creation of large volume percentages of grain boundaries and sub-grain boundaries, and the preferential occurrence of nucleation at the grain boundaries. Fig. 2 shows SEM micrographs taken from BST films deposited on a Si (1 0 0) substrate at 845 °C for 10 h (Fig. 2a) and 30 h (Fig. 2b). The film thicknesses of these two films are 1.1 and 2.8 μm, respectively. It is found from Fig. 1 and Fig. 2 that at the late deposition stage the growth eventually leads to grain impingement and coalescence, with the development of a continuous film with pores at grain boundaries, and that numerous grains nucleate and grow preferentially at the grain boundaries, which may be attributed to the strong binding energy of the absorbed single atoms and the imperfections of the substrate [29]. The second layer of BST film grows over the grains formed, leading to a relatively smooth surface and a well developed microstructure of thick films. This tendency results in an increase in planar grain density and in a decrease in average grain size with film thickness. The average lateral grain size for the film deposited at early stage was directly measured on film photomicrographs using a LADD microcomputer image analyser and the grain size is in the range 1–20 μm. The average grain sizes for thick films, obtained from XRD analysis, are 51.7, 39.9, and 35.4 nm for 0.6, 1.1, and 2.8 μm thick films, respectively. The grain size decreases very quickly in the initial stage to several tens of nanometres, resulting in a failure to observe the columnar structure of the films. These results are consistent with the morphological analysis for BST films.

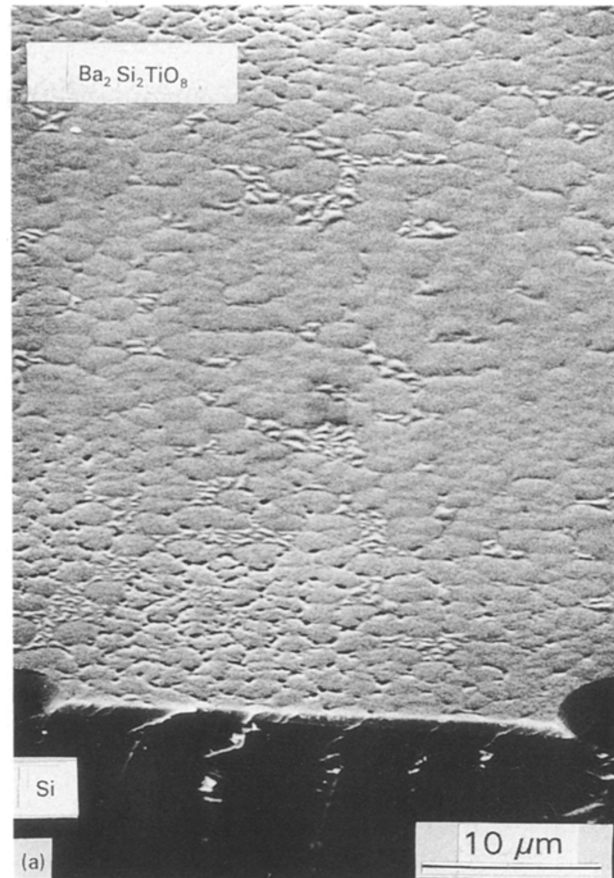

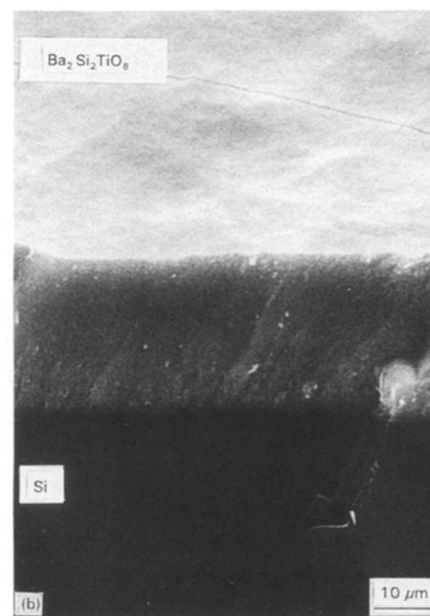

Figure 2 SEM micrographs taken from BST films deposited on a Si (1 0 0) substrate at 845 °C for: (a) 10 h, and (b) 30 h.

3.3. Dependence of film orientation on substrate temperature

Fig. 3 shows XRD patterns recorded from a randomly oriented, polycrystalline BST target and films deposited for 5 h at 750, 822, and 845 °C. Fig. 4 is an XRD spectrum recorded from a 2.8 μm thick film deposited at 845 °C for 30 h. The results of the X-ray analysis indicate that the 1.1 μm thick film grown at an optimum substrate temperature of 845 °C is highly (0 0 1) oriented. It is evident that the film orientation is strongly manipulated by the T_s under the current deposition conditions. For instance, films deposited below 750 °C are amorphous, films deposited at 786 °C < T_s < 822 °C have, more or less, randomly oriented structures, while those films deposited at T_s > 860 °C revealed orientations other than (0 0 1) [17]. The influence of T_s on the (0 0 1) orientation is summarized in Fig. 5, which displays the relative X-ray intensity ratio $I(0\,0\,1)/I(2\,1\,1)$ for films deposited at various substrate temperatures (786 to 865 °C) and sputtering times (5, 10, and 30 h). It is evident that 845 °C is the optimum deposition temperature to grow the (0 0 1)-oriented BST film. The (0 0 1) orientation decreases with sputtering time, hence with the film thickness. For example, the XRD intensity ratio, $I(0\,0\,1)/I(2\,1\,1)$ is 12.8 for the 1.1 μm thick film and reduces to 4.9 for the 2.8 μm thick film, due to the decrease in film-surface temperature with film thickness [15] and to the deviation of the film composition from stoichiometry [14, 15]. Fig. 5 also indicates that high (0 0 1) orientation occurs in a narrow temperature region, and that the longer the sputtering time, the narrower the temperature region, which adds to the difficulties in the preparation of the *c*-axis-oriented BST thin films with a desired thickness for the SAW devices.

3.4. Dependence of film orientation on supersaturation

In a physical deposition, the supersaturation (see Section 1) is an important comprehensive parameter representing the effect of the environment on the deposition rate. Many factors can affect the deposition

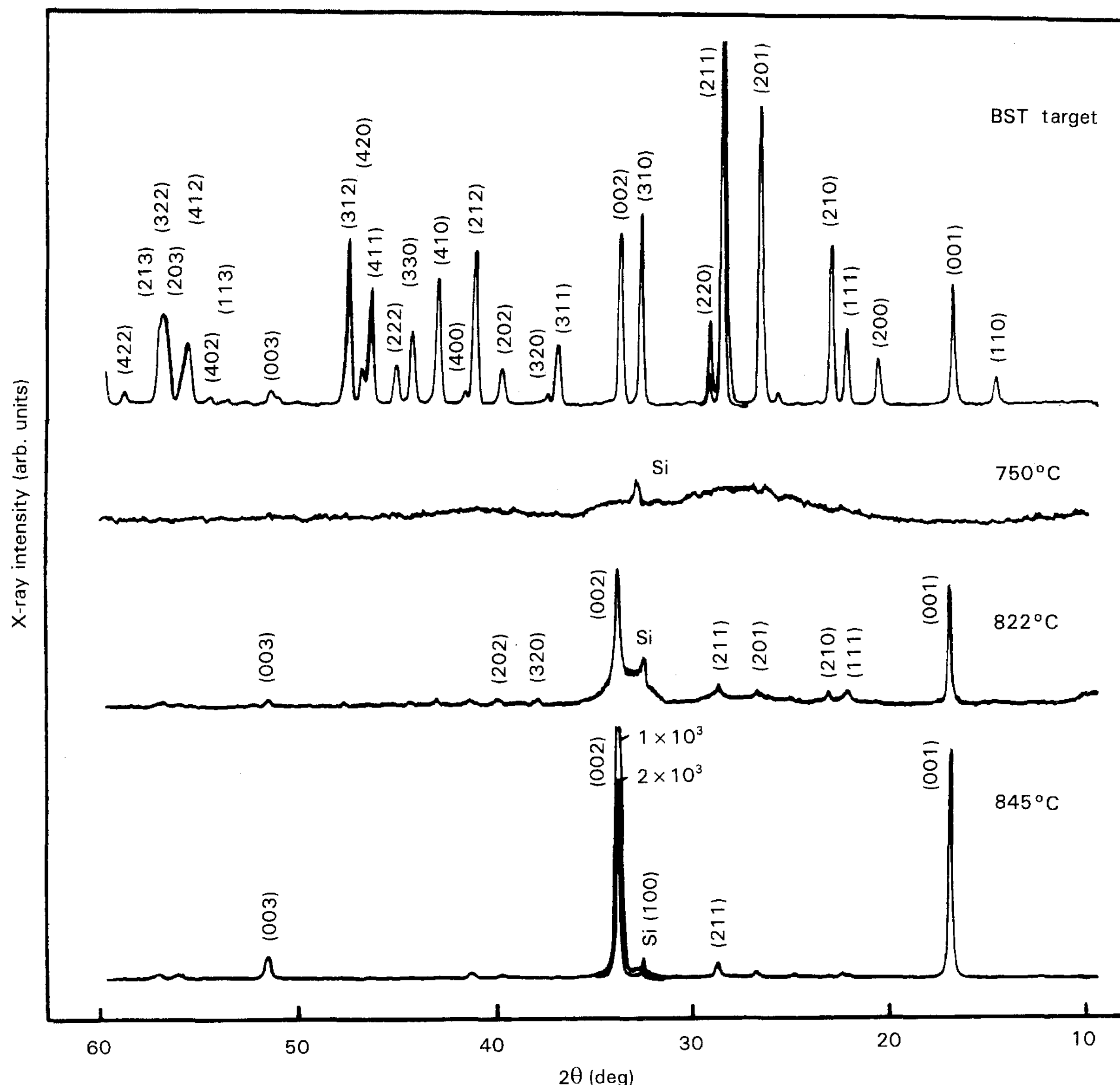

Figure 3 XRD spectra for a BST ceramic target and thin films deposited on Si (1 0 0) substrates for 5 h at 750, 822, and 845 °C.

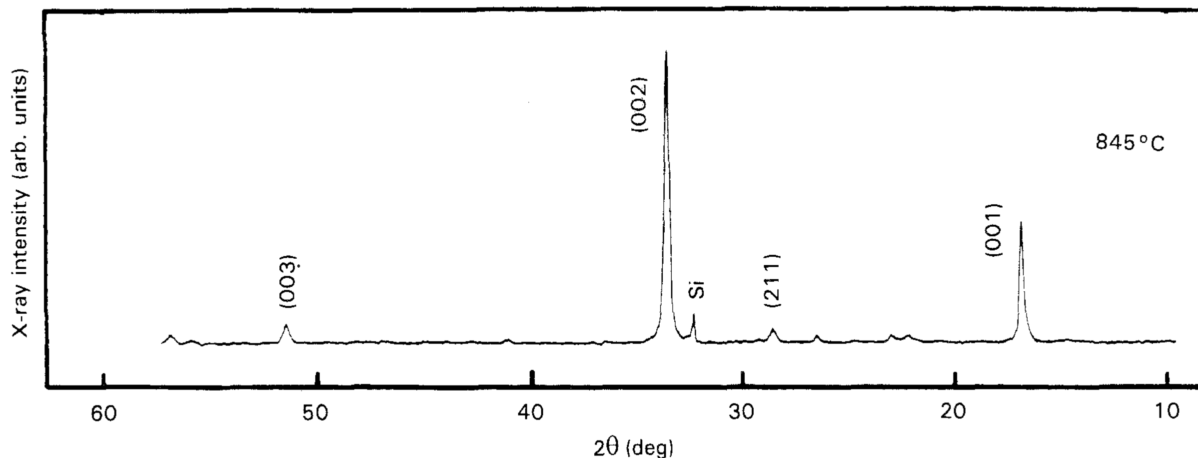

Figure 4 An XRD spectrum for the BST thin film deposited on a Si (1 0 0) substrates for 30 hours at a substrate temperature of 845 °C.

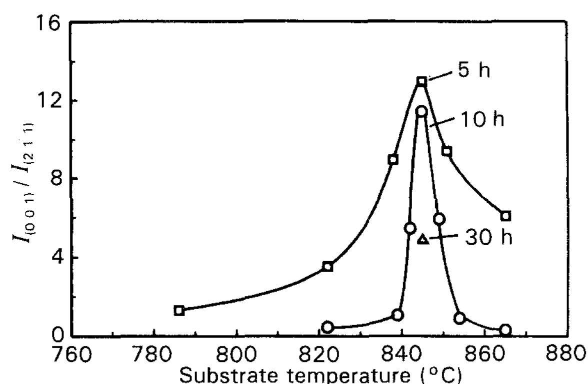

Figure 5 XRD intensity ratios (of (0 0 1) planes to (2 1 1) planes) for BST films grown at various temperatures for 5, 10 and 30 h.

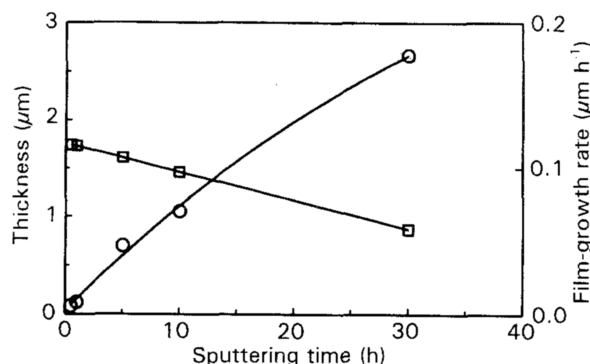

Figure 7 (○) Film thickness and (□) growth rate versus sputtering time at 845 °C. (The initial film-growth rate was 1.95 nm min^{-1}.)

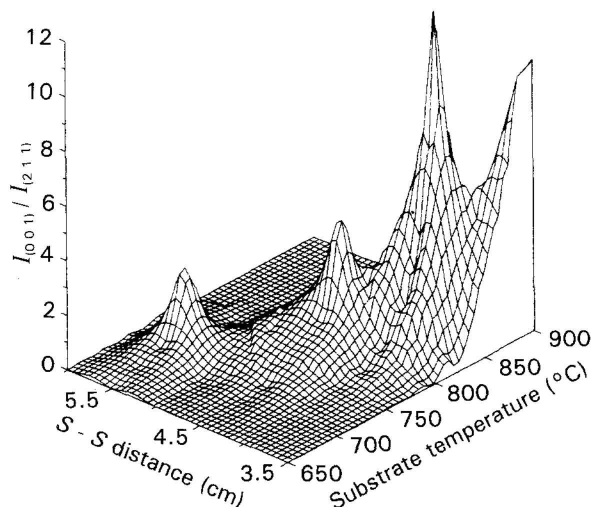

Figure 6 XRD intensity ratios (of (0 0 1) planes to (2 1 1) planes) for BST films deposited at various s–s distances and substrate temperatures.

rate, such as the potential difference between the source and the substrate, the plasma current, the chamber pressure, and the source–substrate (s–s) distance. In this study, as an example, the influence of the s–s distance on the film orientation is introduced. Depositions were carried out for 10 h at various substrate temperatures and at s–s distances of 6.0, 4.5, 4.0, and 3.5 cm. Fig. 6 shows the relative XRD intensity, $I(0\,0\,1)/I(2\,1\,1)$, of the films deposited at various s–s distances. It is evident that the optimum temperature for (0 0 1) orientation shifts from low to high temperature as the s–s distance decreases. The optimum substrate temperature for (0 0 1) orientation is 725 °C for the film deposited at an s–s distance of 5.5 cm, and is 845 °C for the film grown at 4.0 cm. At 725 °C, the film grown at the s–s distance of 4.0 cm has an amorphous structure. A decrease in the s–s distance results in an increase in deposition rate, and hence an increase in supersaturation. According to the capillarity theory (see Equation 2), to retain a nucleation rate, J_2, of a favourable orientation, the substrate temperature must be raised to promote the desorption rate of the adatoms, that is, to decrease the supersaturation and recover the equilibrium conditions favouring the orientation of interest. Therefore, the orientation–substrate temperature profile shown in Fig. 5 shifts towards higher temperature as the s–s distance decreases. A similar tendency has also been found for other orientations. A short s–s distance favours the formation of a thick film, but is usually unfavourable for an optimum texture and adds to the difficulties in the experimental conditions and in the post-cooling process of the films. Therefore, a compromise between the film-growth rate and the film orientation is often required.

3.5. Film-growth kinetics

Cross-sectional SEM micrographs of samples were used to determine the film thickness. Fig. 7 shows the variation of film thickness and film-growth rate in the direction normal to the substrate plane with sputtering time. The average film-growth rate was 1.95 nm min^{-1} at the initial stage, and decreased with sputtering time. The reduction of film-growth rate with time may be attributed to a few factors. The first is the possible decrease in film-surface temperature with increasing film thickness due to the poor thermal conductivity of the BST lattice. A decrease in the surface temperature may promote the nucleation rate and result in a thin and more uniform film [30]. Film orientation is also sensitive to the film-surface temperature. Fig. 5 shows that for the film deposited for 10 h, a temperature decrease of 4 °C from 845 °C caused a relative reduction of 91% in (0 0 1) orientation. At substrate temperatures lower than 845 °C, a randomized structure forms. In this study, the substrate-temperature dependence of the film-growth rate was also studied in a group of films deposited for the same sputtering time, 10 h, at substrate temperatures of 786, 822, 845, and 865 °C. The corresponding film thicknesses are 0.88, 0.95, 1.10, and 1.19 μm, respectively, which is consistent with the analysis above. Another possible reason for the reduction of the film-growth rate may be related to the deviation in chemical composition from stoichiometry with increasing film thickness, as analysed in Section 3.1. of this paper, which altered the grain-growth characteristics and favoured the formation of grains other than (0 0 1) oriented grains and structures other than BST structures.

3.6. Bulk resistivity and surface resistivity

Fig. 8 shows the current–voltage characteristics for 2.8 μm thick BST films deposited at 845 °C; the dependence of the average bulk resistivity at the testing voltage can be obtained. At electric-field strengths lower than 1 kV cm^{-1} (corresponding to a potential difference of 0.3 V between two electrodes), the current-voltage relation is approximately linear, giving a room-temperature bulk resistivity of 1.8×10^7 Ω m. At field strengths higher than 1 kV cm^{-1}, the electric current monotonically increases with voltage (probably due to a tunnelling process at high field strength). When the Au electrode is at positive potential, the current is higher than it is when the Au electrode is at negative potential, which may be attributed to the different electron-injection abilities of Au and Si [31].

The room-temperature bulk resistivity of BST films along the direction of thickness is higher than that of normal metals by 13 orders of magnitude, and higher than that of doped silicon by about nine orders of magnitude. However, it is lower than the resistivities of some dielectric materials such as $BaTiO_3$ (1×10^{12} Ω m [32]). BST is a dielectric material. The lower bulk resistivity of the BST films probably results from the incorporation of minor impurities during sputtering, which is beyond the sensitivity of the WDS method.

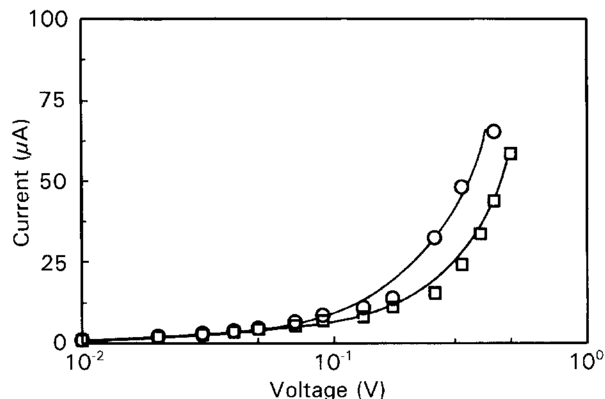

Figure 8 Voltage–current characteristics of a Si–BST–Au electrode system: (○) Au (+), Si (−), and (□) Au (−), Si (+).

At room temperature the average surface resistivity of the BST films deposited at 845 °C is 1.5×10^3 Ω m and it is of isotropic characteristic. Generally, the surface resistivity of an as-deposited film should be higher than the resistivity in the thickness direction due to the columnar grain boundaries. However, the surface resistivity of BST films is lower than the resistivity in the direction normal to the surface, which may be attributed to surface contamination, or to the parallel bulk current inside the film and the parallel current through the silicon wafer [33, 34]. On the other hand, anisotropic surface resistivity is generally expected for single crystalline BST films. The absence of surface-resistivity anisotropy in this study is probably due to the numerous irregular grain boundaries of the (0 0 1) oriented grains.

3.7. High-frequency dielectric properties

The average relative dielectric constant for the film deposited at 845 °C is 2.828 at the testing frequency 1 MHz, and decreases to 0.959 at 5 MHz. For frequencies higher than 9 MHz, the dielectric constants are less than 0.05 in all cases. The room-temperature dielectric constant of a BST single crystal was reported as 11.0 at 1 kHz [5]. Thus the measured dielectric constants of the BST thin films are therefore reasonable. Compared to the dielectric constants of typical piezoelectric materials (such as 4.6 for α-quartz [35], 38.7 for $Bi_{12}GeO_{20}$ [36], 41.0–44.0 for $LiNbO_3$ [37], and 425–3400 for Pb(Zr, Ti)O_3 [38], the dielectric constant of BST films is very low and is favoured for SAW applications.

The dielectric loss for a 2.8 μm thick BST film deposited at 845 °C (sample TF52) was measured at frequencies from 1 to 500 MHz and is shown in Fig. 9. For some narrow frequency ranges, the dielectric loss increases from 10 to 38, while for most of the frequency band the loss is lower than 1.0. The high-frequency impedance for the film is also displayed in Fig. 9. Some segments of the impedance curve show an "S" shape rotated by 90°. The lowest value of the impedances is 15.0 Ω measured at 9 MHz. The phase angle of impedance is − 48.5° at 1 MHz, + 8.6° at 10 MHz, and passes through 0° at about 9.5 MHz. The 90°-rotated "S" shape of the impedance curve

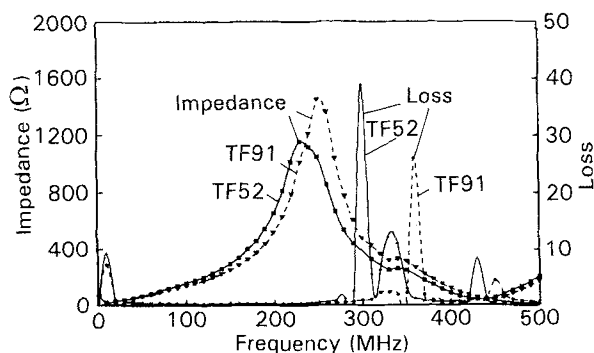

Figure 9 Frequency dependence of dielectric loss and impedance for 2.8 μm thick BST films deposited at 845 °C.

shown in Fig. 9 is characteristic of the impedance curve for an unloaded piezoelectric resonator [39]. A piezoelectric sample under testing can be treated electrically as a serial equivalent circuit that is made up of a resistance, an inductance, and a capacitance. When the impedance of the equivalent circuit, Z, is minimum, the output of the circuit is maximum, and the corresponding frequency is defined as the minimum-impedance frequency [39], which is one of the characteristic frequencies determining the principal SAW parameters of a thin-film device. For BST films the minimum-impedance frequency is 9 MHz. Another characteristic value in the SAW technique is the serial resonant frequency which is defined as the frequency when the phase angle of the serial circuit is equal to zero and the circuit is in a resonant state. For BST films, the serial resonant frequency is about 9.5 MHz.

In this study, the multiple-peak phenomenon of the dielectric-loss curve (see Fig. 9) was analysed by comparing the impedance spectra and dielectric-loss spectra recorded from several film specimens of different orientation degree. For example, the spectra taken from two BST films with ratios $I(0\,0\,1)/I(2\,1\,0)$ of 4.2 (sample TF52) and 3.9 (sample TF91) are displayed in Fig. 9. The positions of the first peak for both dielectric-loss curves are all at 9 MHz, and the two impedance curves also coincide at 9 MHz, which indicates that the dielectric loss measured at this frequency is the result of an intrinsic process and is probably caused by a resonant movement of the dielectric BST lattices.

A frequency shift for both of the impedance peaks and the dielectric-loss peaks at frequencies higher than 100 MHz is evident in Fig. 9. It is well known in dielectric physics that in an alternating current (a.c.) electric field the variation in dielectric loss indicates a relaxation process of the material structure [40, 41]. Dielectric relaxation is featured by the electric-dipole model [42] and the space-charge model [41] in many solid dielectric materials, and also by the elastic-dipole mechanism in piezoelectric materials [43]. In the sputtered thin films, the dielectric dipoles could be impurities, badly-oriented crystal units, and other non-stoichiometric components having dipole moments. All of these factors would contribute to the dielectric loss of thin films and complicate the frequency spectra. Even though the dielectric loss-frequency relation shown in Fig. 9 indicates the frequency regions that are suitable for SAW devices.

4. Conclusion

High c-axis oriented polycrystalline $Ba_2Si_2TiO_8$ thin films, with a thickness up to 2.8 μm, have been successfully grown on Si (1 0 0) substrates using a r.f.-sputter technique. The chemical composition of BST ceramic targets is almost stoichiometric, while the compositions of films increasingly deviate from stoichiometry with film thickness. The grain morphology is dependent on the substrate texture. At the initial stage of deposition the BST grains deposited on the HF etched SI (1 0 0) substrate align along the Si substrate lattices, grow into two-dimensional polygonal shapes, and have a non-liquid-like-coalescence characteristic. The average grain size decreases quickly with film thickness, resulting in a relatively dense structure and the smooth surface of the thicker films. X-ray analysis indicates a substrate-temperature region from 822 to 865 °C and an optimum substrate temperature of 845 °C for growing (0 0 1) oriented BST thin films under the current experimental conditions. The film orientation is manipulated by the substrate temperature and the supersaturation. At 845 °C the film growth rate is 1.95 nm min^{-1} in the initial stage of deposition, and decreases with film thickness due to the decrease in film-surface temperature and to the compositional deviation from stoichiometry during the sputtering. The average room-temperature bulk resistivity of BST films deposited at 845 °C is of the order $10^7\ \Omega$m, and the average surface resistivity of the films is isotropic and of the order $10^3\ \Omega$m. BST films have dielectric constants lower than 0.05 at frequencies higher than 9 MHz, dielectric losses less than 0.05 in most parts of the frequency band from 1 to 500 MHz, and high-frequency impedance characteristics that are typical of piezoelectric materials.

Acknowledgements

The authors would like to thank Dr W. V. Youdelis and Dr D. O. Northwood at the University of Windsor for helpful discussions. Thanks are also extended to Mr A. R. Chan, Mr R. Paparella and Mr D. A. Pawlik in ECD for their technical assistance with SEM and XRD measurements.

References

1. J. T. ALFORS, M. C. STINSON, R. A. MATTHEWS and A. PABST, *The American Mineralogist* **50** (1965) 314.
2. R. MASSE, J. C. GRENIER and A. DURIF, *Bull. Soc. fr Minéral. Cristallogr.* NC (1967) 20.
3. M. KIMURA, Y. FUINO and T. KAWAMURA, *Appl. Phys. Lett.* **29** (1967) 227.
4. M. KIMURA, *J. Appl. Phys.* **48** (1977) 2850.
5. A. HALLIYAL, A. S. BHALLA, S. A. MARKGRAF, L. E. GROSS and R. E. NEWNHAM, *Ferroelectrics* **62** (1985) 27.
6. J. MELNGALIS, J. F. VETELINO, A. JHUNJHUNWALA, T. B. REED, R. E. FAHEY and E. STERN, *Appl. Phys. Lett.* **32** (1978) 203.
7. H. YAMAUCHI, *J. Appl. Phys.* **49** (1978) 6162.

8. G. R. BARSH and R. E. NEWNHAM, United States Air Force Report No. AFCRL-TR-75 (1975) 0163.
9. H. YAMAUCHI, K. YAMASHITA and H. TAKAUCHI, *J. Appl. Phys.* **50** (1979) 3160.
10. K. TSUBOUCHI, K. SUGAI and N. MIKOSHIBA, in Proceedings of the Ultrasonic Symposium Vol. 1, November 5–7, 1980, Boston, MA, edited by B. R. McAvoy (IEEE, New York, 1980) p. 446.
11. H. YAMAUCHI, R. J. WHITE, M. AYUKAWA, T. C. MARRAY and J. W. ROBINSON, *J. Mater. Res.* **3** (1988) 105.
12. R. J. WHITE, M. AYUKAWA, G. DEMAGGIO, J. W. ROBINSON and M. YAMAUCHI, in "High Tech ceramics", edited by P. Vincenzini (Elsevier Science, Amsterdam, 1987) p. 657.
13. P. M. KAWA, C-axis Oriented $Ba_2Si_2TiO_8$ Thin Films, M.S. thesis, University of Windsor, Ontario, Canada (1988) p. 1.
14. Y. LI, B. S. CHAO and H. YAMAUCHI, in Proceedings of the Third Canadian Material Science Conference, June 18–21, 1991, Kingston, Ontario (Royal Military College of Canada, 1991) p. 10.
15. Y. LI, B. S. CHAO and H. YAMAUCHI, *J. Appl. Phys.* **71** (1992) 4903.
16. *Idem*, 'Effect of substrate texture on orientations of rf sputtered $Ba_2Si_2TiO_8$ thin films", unpublished.
17. *Idem, ibid.*
18. L. L. KAZMERSKI, in "Polycrystalline and amorphous thin films and devices" (Academic Press, New York, 1980) p. 4.
19. J. W. MATHEWS, in "Physics of thin films", edited by G. Hass and P. E. Thun, Vol. 4 (Academic Press, New York, 1967) p. 137.
20. J. L. KENTY and J. P. HIRTH, *Surf. Sci.* **15** (1969) 403.
21. H. SATO and S. SHINOZAKI, *Surf. Sci.* **22** (1970) 229.
22. X-ray Powder Diffraction File No. 22–513 (Joint Committee on Powder Diffraction Standards, Swarthmore, PA, 1972).
23. S. O. HYATT, "Reactive sputtered TiN thin films for diffusion barriers", PhD dissertation, University of Windsor, Ontario, Canada (1990) p. 40.
24. L. I. MAISSEL, in "Handbook of thin film technology", edited by L. I. Maissel and R. Glang (McGraw-Hill, New York, 1970) p. 13–6.
25. J. L. VOSSEN, *J. Vac. Sci. Tech.* **8** (1971) s12.
26. K. REICHETT and X. JIAN, *Thin Solid Films* **191** (1990) 91.
27. R. J. WHITE, "Fresnoite ceramics and their thin films", M.S. Thesis, University of Windsor, Windsor, Ontario, Canada (1986) p. 125.
28. X-ray Powder Diffraction File No. 5-626 (Joint Committee for Powder Diffraction Standards – JCDD, Swarthmore, PA, 1953).
29. J. P. HIRTH and G. M. POUND, in "Condensation and evaporation: Nucleation and growth kinetics", progress in Materials Science, Vol. 11 (The Macmillan Co, New York, 1963) p. 41.
30. J. A. THORNTON, *Ann. Rev. Mater. Sci.* **7** (1977) 239.
31. J. G. SIMMOS, in "Handbook of thin films technology", edited by L. I. Maissel and R. Glang (McGraw-Hill, New York, 1970) Ch. 14, pp. 14–1.
32. S. IIDA, K. OONO, T. KAMIMAE and H. KUMAGAYA, in "Handbook of physics" (Science Press. Beijing, 1969) p. 138.
33. J. CHEN and Z. LIU, in "Dielectric physics" (Mechanical Industry Press, Beijing, 1982) p. 287.
34. Y. LIU and C. QIU, in "Measurement technique for electrical insulation" (Mechanical Industry Press, Beijing, 1981) p. 43.
35. Y. LI, Z. QIN and Z. ZHOU, in "Measurement of piezoelectric and ferroelectric materials" (Science Press, Beijing, 1984) p. 329.
36. A. J. SLOBODIK and J. C. SETHARES, United States Air Force Report No. AFCAL-71-0570 (1971) 10.
37. T. YAMADA, *Jpn. J. Appl. Phys.* **6** (1967) 151.
38. D. A. BERLINCOURT, in *Proceedings of the National Electronics Conference* Vol. 11 (1955) 777.
39. D. A. BERLINCOURT, D. R. CURRAN and H. JAFFE, in "Physical acoustics", Vol. I, edited by W. P. Mason (Academic Press, New York, 1964) p. 169.
40. V. V. DANIEL, in "Dielectric relaxation" (Academic Press, London, 1967) Ch. 2, p. 13.
41. A. R. VON HIPPEL, in "Dielectric materials and applications", edited by A. R. von Hippel (Technical Press of MIT and John Wiley, New York, 1954) p. 18.
42. H. FRÖHLICH, "Theory of dielectrics" (Clarendon Press, Oxford, 1958) p. 21.
43. A. S. NOWICK and W. R. HELLER, *Adv. in Phys.* **12** (1963) 251.

Received 30 April
and accepted 17 November 1992